


Equilibrium shapes and stability of magnetic filaments

M. Belovs and A. Cēbers 

MMML Laboratory, Department of Physics, University of Latvia, Jelgavas-3, LV-1004 Rīga, Latvia



(Received 2 November 2021; accepted 21 December 2021; published 5 January 2022)

Equilibrium shapes of magnetic rods and their stability under the action of an applied field are analyzed. The family of shapes is characterized by two magnetoelastic numbers due to the remanent magnetization and paramagnetic susceptibility of the rod. Since in experiments with flexible magnetic rods the ends are usually unfixed and unclamped, their stability is analyzed under these conditions. Solutions of the corresponding eigenvalue problems for particular cases show that under these conditions the equilibrium shapes are unstable.

DOI: [10.1103/PhysRevE.105.014601](https://doi.org/10.1103/PhysRevE.105.014601)

I. INTRODUCTION

Flexible magnetic filaments have recently attracted the growing interest of researchers. One of the ways to create them consists of linking functionalized magnetic particles by some linker (biotinized DNA fragments, some polymer) [1,2]. These filaments display certain mechanical instabilities leading to the formation of hairpins [3] in the case of paramagnetic rods or loops [4] in the case of ferromagnetic filaments. Equilibrium solutions for paramagnetic rods with one clamped and one free end under the action of an applied field of various orientations and subjected to various loads are investigated in Ref. [5]. If the symmetry of the filament is broken (by cargo, formation of a hairpin or a loop), then their self-propulsion in an ac field is possible [6]. It should be noted that the numerical simulations have shown that the deformed configurations are unstable [7,8] and for their stabilization some defects of the filament should be introduced (a smaller bending modulus in the central part of the filament). In Ref. [9] ferromagnetic filaments were created by linking ferromagnetic microparticles. These filaments possess several interesting properties such as the formation of loops at inversion of the applied field and their straightening through the third dimension. It should be noted that the problem of a ferromagnetic rod at field inversion is similar to the classical Euler problem of an elastic rod under the action of compressional force. As a result the Euler problem for a rod with paramagnetic properties is analogous to the behavior of a ferromagnetic filament with paramagnetic properties. This problem was considered in Ref. [10]. Its solution in terms of the elliptic Weierstrass function is considered in Ref. [11]. Since in real situations the magnetic filaments are freely floating in some carrier fluid, the appropriate boundary conditions correspond to unfixed and unclamped ends, and a question arises regarding the stability of the equilibrium solutions of this problem.

The equilibrium shapes of the ferromagnetic filaments with paramagnetic susceptibility and their stability are investigated in the present paper. In Sec. II the model is formulated and

a general solution for the equilibrium shapes is given. In Sec. III the parameter space is analyzed and the characteristic solutions for its different regions are given. For an analysis of their stability two algorithms are described, semianalytical and numerical, and their correspondence for the considered values of the parameters is demonstrated. The main conclusions are summarized in Sec. IV and the claim is made that the hairpin and U-like configurations with unfixed and unclamped boundary conditions are unstable.

II. MODEL

The magnetization of the filament according to the hysteresis curve of core-shell ferromagnetic particles used in Ref. [9] consists of two parts—the remanent magnetization and a magnetization due to a finite paramagnetic susceptibility. It should be noted that in a such a setting the problem is isomorphic to the problem of the paramagnetic rod buckling under the action of compressional force. The energy of the filament includes the elastic bending energy and the energy of interaction with an applied field $\vec{H}_0 = (H_0, 0)$,

$$E = \frac{1}{2} \int C_b \left(\frac{d\vartheta}{dl} \right)^2 dl - \frac{b^2(\mu - 1)^2 H_0^2}{8(\mu + 1)} \int \cos^2(\vartheta) dl + MH_0 \int \cos(\vartheta) dl. \quad (1)$$

Here, C_b is the bending modulus, l is the natural parameter of the centerline, b is the radius of the cross section, μ is the paramagnetic permeability, and M is the remanent magnetization of the filament per its unit length. The sign before the third term in relation (1) corresponds to the magnetization $\vec{M} = -M\vec{i}$ ($\vec{i} = [\cos(\vartheta), \sin(\vartheta)]$) is the tangent vector to the centerline of the rod) to emphasize the analogy with the Euler rod under the action of a compressional force. The geometry of the setting is shown by a sketch in Fig. 1.

Minimizing the energy (1) with respect to ϑ the Euler-Lagrange equation reads

$$-C_b \frac{d^2\vartheta}{dl^2} + \frac{b^2(\mu - 1)^2 H_0^2}{8(\mu + 1)} \sin(2\vartheta) - MH_0 \sin(\vartheta) = 0. \quad (2)$$

*aceb@tesla.sal.lv

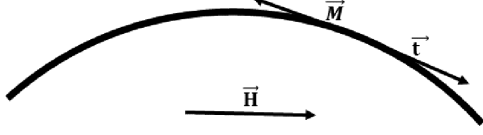


FIG. 1. Sketch of the ferromagnetic rod with the magnetization antiparallel to an applied field.

Scaling the natural parameter l by the characteristic length $\lambda = \sqrt{C_b/(MH_0)}$ and introducing two magnetoelastic numbers $Cm_p = \frac{b^2(\mu-1)^2H_0^2L^2}{8(\mu+1)C_b}$ and $Cm_f = \frac{MH_0L^2}{C_b}$ ($2L$ is the length of the rod), Eq. (2) may be put in the following dimensionless form:

$$\frac{d^2\vartheta}{dl^2} + \sin(\vartheta) - \frac{Cm_p}{Cm_f} \sin(2\vartheta) = 0. \quad (3)$$

Equation (3) has the first integral,

$$a^2 \left(\frac{d\vartheta}{dl} \right)^2 + [\cos(\vartheta) - a^2]^2 = c^2, \quad (4)$$

where c is the integration constant and $a^2 = \frac{Cm_f}{2Cm_p}$. Introducing the variable $z = \cos(\vartheta)$, Eq. (4) is put in the following form:

$$a^2 \left(\frac{dz}{dl} \right)^2 = (1 - z^2)[c^2 - (z - a^2)^2]. \quad (5)$$

The roots of the fourth-order polynomial on the right-hand side of Eq. (5) are denoted as $\alpha_1 < \alpha_2 < \alpha_3 < \alpha_4$. The solution of Eq. (5) according to Ref. [10] is found by using the substitution

$$\frac{z - \alpha_2}{z - \alpha_3} = p \frac{t + 1}{t - 1}, \quad (6)$$

which gives

$$4a^2 \left(\frac{dt}{dl} \right)^2 = B^2(1 - t^2) \left(1 - \frac{1}{h^2}t^2 \right). \quad (7)$$

The solution of Eq. (7) is found in terms of the Jacobi elliptic function $t = \text{sn}(\frac{B}{2a}l, \frac{1}{h})$. The following notations are introduced:

$$\begin{aligned} p^2 &= \frac{(\alpha_1 - \alpha_2)(\alpha_4 - \alpha_2)}{(\alpha_1 - \alpha_3)(\alpha_4 - \alpha_3)}, \\ B &= \sqrt{\alpha_2 - \alpha_1} \sqrt{\alpha_4 - \alpha_3} + \sqrt{\alpha_3 - \alpha_1} \sqrt{\alpha_4 - \alpha_2} > 0, \\ h &= \frac{B^2}{(\alpha_3 - \alpha_1)(\alpha_4 - \alpha_2) - (\alpha_2 - \alpha_1)(\alpha_4 - \alpha_3)} > 1. \end{aligned} \quad (8)$$

The solution of Eq. (7) then gives

$$\cos(\vartheta) = \alpha_3 + \frac{(\alpha_3 - \alpha_2) \left[\text{sn}\left(\frac{B}{2a}l, \frac{1}{h}\right) - 1 \right]}{(p - 1) \text{sn}\left(\frac{B}{2a}l, \frac{1}{h}\right) + p + 1}. \quad (9)$$

The configurations are found by integration of the set of ordinary differential equations (ODEs),

$$\frac{dx}{dl} = \cos[\vartheta(l)], \quad \frac{dy}{dl} = \sin[\vartheta(l)]. \quad (10)$$

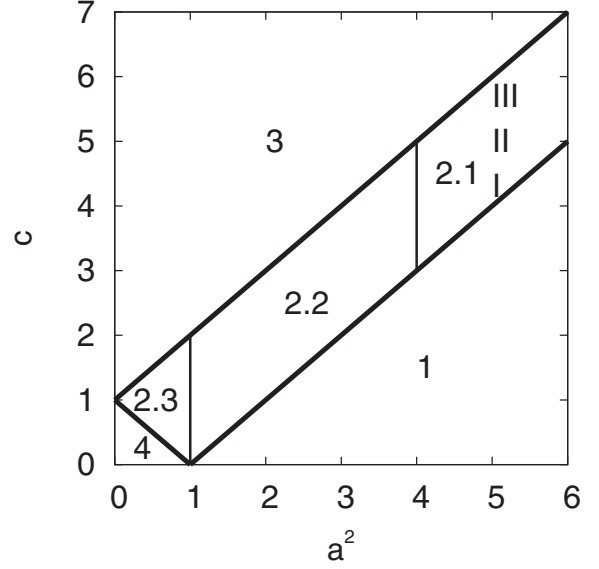


FIG. 2. Regions in parameter space.

III. EQUILIBRIUM SHAPES AND THEIR STABILITY

In the parameter space (a^2, c) the four regions shown in Fig. 2 are considered. In regions 1 and 3 neutral solutions do not exist. On the boundaries between regions 1–4 the fourth-order polynomial has double roots. On the boundary $c = 1 + a^2$ the tangent angle approaches $\vartheta = \pi$ as $l \rightarrow \pm\infty$. For this solution only the permanent magnetic moment in the loop is opposite to the magnetic field direction. By integration of Eq. (5) in this case an analytical solution is available [10],

$$\cos[\vartheta(l)] = \frac{(1 + 2a^2) \tanh^2(\sqrt{1 + a^2}l/a) - (1 + a^2)}{\tanh^2(\sqrt{1 + a^2}l/a) - (1 + a^2)}. \quad (11)$$

The shape of the rod corresponding to the tangent angle given by (11) is shown in Fig. 3. In Ref. [10] it is found that the solution (11) is unstable with respect to the loop migration

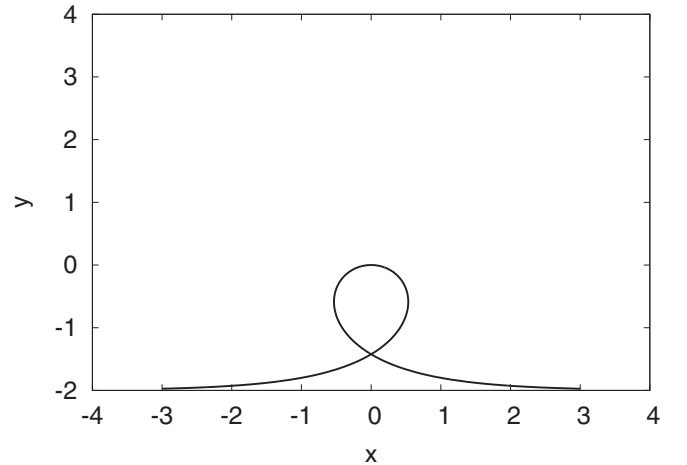
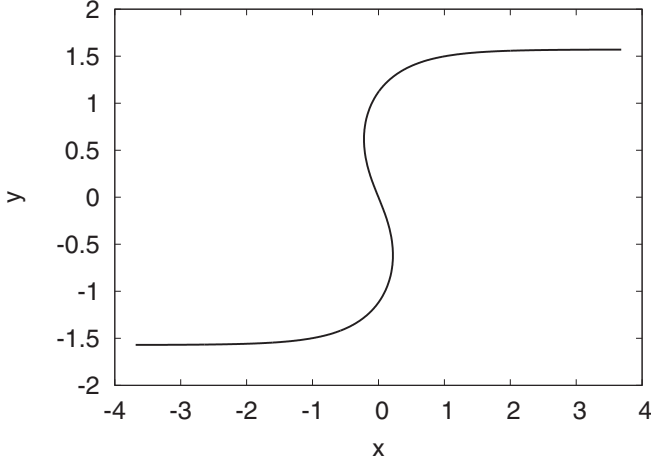


FIG. 3. Loop solution on the boundary between regions 2 and 3 at $a = 100$.

FIG. 4. Kink at $a = 0.5$.

towards one of the ends of the rod. In Ref. [9] it is shown that the loop with a finite length is unstable also with respect to the three-dimensional perturbation leading to the straight rod.

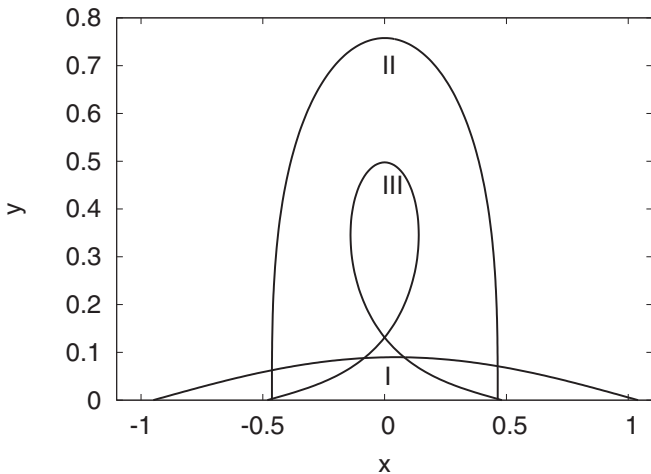
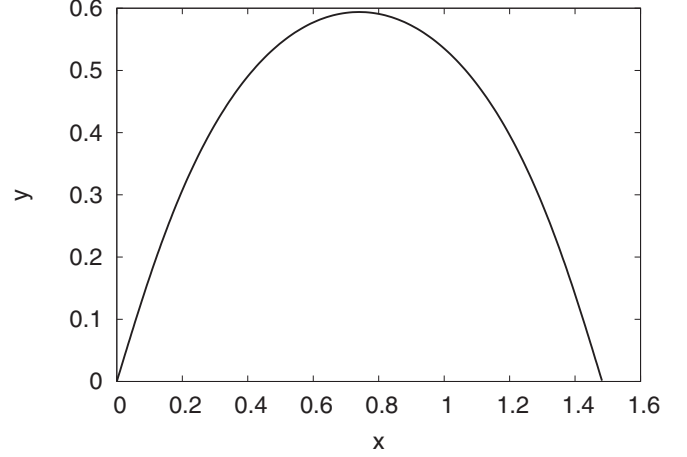
On the boundary $c = -1 + a^2$ the only solutions possible are $z = \pm 1$ [$\cos(\vartheta) = \pm 1$] and these correspond to the permanent moment along the field ($\vartheta = \pi$) and opposite to it. Only the first one is stable, of course.

On the boundary between regions 2 and 4 the fourth-order polynomial has the double root $z = 1$. In this case the limiting shape is different than the one shown in Fig. 3. Integration of Eq. (5) in this case ($c = 1 - a^2$) gives

$$\cos(\vartheta) = 1 - \frac{4(1 - a^2)}{a^2[\cosh(2\sqrt{1 - a^2}l/a) + 1] + 2}. \quad (12)$$

The shape of the filament corresponding to the tangent angle given by the relation (12) at $a = 0.5$ is shown in Fig. 4. Concerning the solution Eq. (12) we may note that the boundary conditions $d\vartheta/dl = 0$ are satisfied also by the semi-infinite solutions $l \in (-\infty, 0)$ and $l \in (0, \infty)$.

In region 2 U-like solutions exist and in region 4 hairpins. Figure 5 shows the metamorphosis of the shapes as the pa-

FIG. 5. Metamorphosis of shapes in region 2 for the sequence of parameters shown in Fig. 2 ($a^2 = 5$; $c = 4.01, 5, 5.99$).FIG. 6. Neutral solution at $Cm_f = 2.842$, $Cm_p = 1.421 \times 10^{-4}$.

rameter c in region 2 transitions from the lower boundary to the upper one. Starting from a weakly bent shape at the lower boundary the shape transforms to the loop as it approaches the upper boundary. Qualitatively similar behavior is characteristic for all a values in region 2.

In the case $a \rightarrow \infty$ ($Cm_p \rightarrow 0$) in region 2 the neutral solution approaches the U-like shape, as is characteristic for the ferromagnetic rod.

In region 2 (Fig. 2) the roots of the fourth-order polynomial are ordered as follows: $\alpha_1 = -1 < \alpha_2 = a^2 - c < \alpha_3 = 1 < \alpha_4 = a^2 + c$. In regions 2.1 and 2.2, which correspond to $-1 + a^2 < c < 1 + a^2$ and $a > 1$, the following parametrization is introduced, $c = a^2 - \cos(\gamma)$, $\gamma \in (0, \pi)$, which gives ($\tau = 1/a^2$)

$$b(\gamma, \tau) = \frac{B(c, a)}{2a} = \sqrt{1 - \tau \cos(\gamma)} + \cos(\gamma/2) \sqrt{1 - \tau \cos^2(\gamma/2)},$$

$$k(\gamma, \tau) = 1/h(c, a) = \frac{\sin^2(\gamma/2)}{b^2(\gamma, \tau)} [1 + \tau \sin]. \quad (13)$$

At the unclamped end points the boundary condition is satisfied at $\cos(\vartheta) = a^2 - c$ when $\text{sn}[b(\gamma, \tau)l, k(\gamma, \tau)] = -1$. Rescaling the arc length according to $\tilde{l} = l\sqrt{Cm_f}/L$ ($2L$ is the length of the rod, and hereinafter the tildes are omitted) we obtain the following condition for the magnetoelastic number Cm_f :

$$\sqrt{Cm_f} = \frac{2K[k(\gamma, \tau)]}{b(\gamma, \tau)} = f_1(\gamma, \tau). \quad (14)$$

The function $f_1(\gamma, \tau)$ at fixed $\tau \in (0, 1/4)$ ($a > 2$) increases monotonically with γ from its minimal value $f_1|_{\gamma=0} = \frac{\pi}{2\sqrt{1-\tau}}$. As a result a nontrivial neutral solution exists at $Cm_f > Cm_f^c = \frac{\pi^2 a^2}{4(1-a^2)}$. Its solution in the limit $Cm_p \rightarrow 0$ gives $Cm_f^c = \frac{\pi^2}{4} + 2Cm_p$ —the paramagnetic susceptibility of the rod stabilizes it with respect to the formation of the U-like configuration. An example of a neutral configuration at $Cm_f = 2.842$, $Cm_p = 1.421 \times 10^{-4}$ is shown in Fig. 6.

Further, we consider the stability of the neutral solutions we have obtained. This is studied by two different methods,

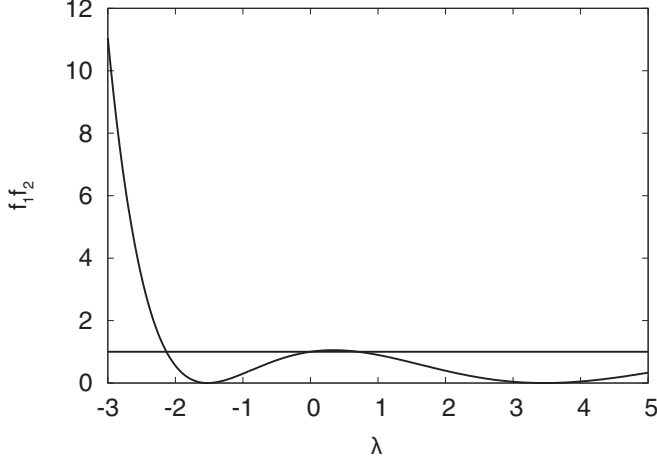


FIG. 7. Solution of eigenvalue problem at $Cm_f = 2.842$, $Cm_p = 1.421 \times 10^{-4}$. The intersection point of the horizontal line and $f_1(\lambda)f_2(\lambda)$ curve gives the eigenvalues.

one semianalytical and the other numerical. The second variation of the energy (dimensionless) at neutral solution $\vartheta_0(l)$ reads (the arc length is scaled by L)

$$\delta^2 E = \int_{-1}^1 \left[\left(\frac{d\delta\vartheta}{dl} \right)^2 + [2Cm_p \cos(2\vartheta_0) - Cm_f \cos(\vartheta_0)] \delta\vartheta^2 \right] dl. \quad (15)$$

If the eigenvalue problem [here, $Q(l) = 2Cm_p \cos(2\vartheta_0) - Cm_f \cos(\vartheta_0)$]

$$-\frac{d^2\delta\vartheta}{dl^2} + Q(l)\delta\vartheta = \lambda\delta\vartheta, \quad \left. \frac{d\delta\vartheta}{dl} \right|_{l=\pm 1} = 0, \quad (16)$$

has a negative eigenvalue, then the neutral solution is unstable. The first method of the solution of the spectral problem (16) is similar to the well-known shooting method and is as follows. The eigenvalues are the roots of the equation

$$f_p(\lambda)f_m(\lambda) = 1, \quad (17)$$

where $f_p(\lambda) = h_p(1, \lambda)$ and $h_p(l, \lambda)$ is the solution of the Cauchy problem,

$$-\frac{d^2 h_p}{dl^2} + Q h_p = \lambda h_p, \quad h_p(-1, \lambda) = 1, \quad \frac{dh_p}{dl}(-1, \lambda) = 0, \quad (18)$$

and $f_m(\lambda) = h_m(-1, \lambda)$, where $h_m(l, \lambda)$ is the solution of the Cauchy problem,

$$-\frac{d^2 h_m}{dl^2} + Q h_m = \lambda h_m, \quad h_m(1, \lambda) = 1, \quad \frac{dh_m}{dl}(1, \lambda) = 0. \quad (19)$$

Details of the derivation of Eq. (17) are given in the Appendix.

In the case of the numerical example considered above ($Cm_f = 2.842$, $Cm_p = 1.421 \times 10^{-4}$) from Fig. 7 we see that there is one negative eigenvalue, -2.13 . Thus the U-like neutral solution of the ferromagnetic rod is unstable.

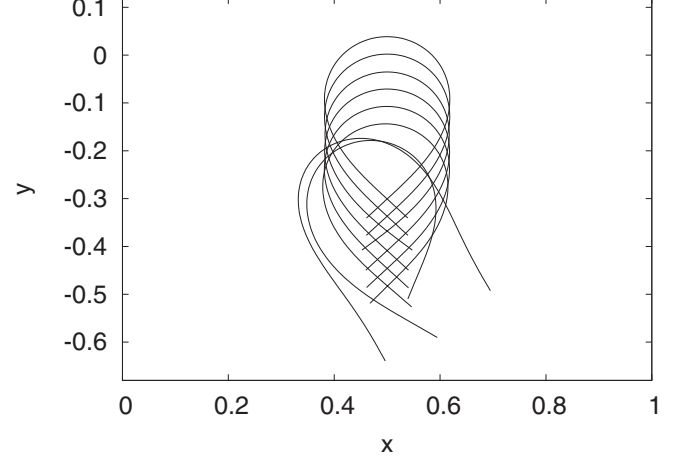


FIG. 8. Instability of oscillating and propelling a filament with a U-like shape. $Cm_f = 3.75$, $T/\tau_e = 0.16$.

In another approach the eigenvalue problem is solved by discretization Eq. (20) with finite differences,

$$\frac{d^2 \delta\vartheta}{dl^2} - Q(l)\delta\vartheta = \lambda\delta\vartheta, \quad (20)$$

and calculation of the eigenvalues of the arising matrix. The mesh in the interval $[-1, 1]$ $l_i = -1 + (i-1)h_1$ ($i = 1, \dots, n+1$) ($h_1 = 2/n$ is the mesh size) is introduced and the matrix A constructed: $A(i, i) = -2/h_1^2 - Q(l_i)$, $A(i, i+1) = 1/h_1^2$, $A(i, i-1) = 1/h_1^2$ ($i = 2, \dots, n$) and $A(1, 1) = 1$, $A(1, 2) = -1$, $A(n+1, n+1) = 1$, $A(n+1, n) = -1$. To satisfy the boundary conditions the matrix B is introduced, $B(i, i) = 1$ ($i = 2, \dots, n$), $B(1, 1) = 0$, $B(n+1, n+1) = 0$, and eigenvalues are found from the general eigenvalue problem $Ax = \lambda Bx$. In the case of the numerical example considered above ($Cm_f = 2.842$, $Cm_p = 1.421 \times 10^{-4}$) the calculated negative eigenvalue [$\lambda = -2.13$ ($n = 300$)] coincides with the one calculated by the first method. The numerical method is indispensable, for example, for the analysis of the Euler problem of the stability of the neutral solution for the rod with clamped and fixed ends when it is necessary to account for the constraint. The corresponding calculation shows that at these boundary conditions the neutral solution corresponding to the first mode is stable. It is interesting to note that higher modes of the Euler problem are unstable.

The conclusion regarding the instability of the ferromagnetic rod with the free and unclamped ends is in agreement with the experimental observations in Ref. [12], where it is found that in order to achieve a stable self-propulsion of the ferromagnetic rod in the piecewise pulsed magnetic field, the time duration of the unstable situation should be chosen sufficiently small. It should be noted as well that the U-like shape leading to the formation of the loop is also unstable with respect to the three-dimensional perturbations as shown in Ref. [9] and is not considered by the present approach.

The characteristic sequence of events at the development of the instability of a U-like shape in a pulsed field, observed in the experiments [12], is shown in Fig. 8 by the dynamics of the ferromagnetic rod obtained numerically at $Cm_f = 7.75$ and $T/\tau_e = 0.16$, where T is the period of pulsed field and

$\tau_e = \zeta L^4 / C_b$ is the characteristic elastic relaxation time. A numerical simulation shows that oscillating and propelling a filament with a U-like shape (shown for several periods in Fig. 8) is unstable with respect to the elongation of one of its legs and a shortening of another, which corresponds to the development of the instability mode described above. Due to this instability the filament overturns to the stable orientation and the propulsion stops.

As the second example of the study of the stability of the neutral equilibrium solutions, we consider the case $a \rightarrow 0$ which corresponds to the hairpins of the paramagnetic rods under the action of the magnetic field perpendicular to the initially straight rod. It corresponds to region 4 in the parameter space (a^2, c) shown Fig. 1. In this case the sequence of the roots of the fourth-order polynomial is as follows: $\alpha_1 = -1$, $\alpha_2 = a^2 - c$, $\alpha_3 = a^2 + c$, $\alpha_4 = 1$. In this case the relations corresponding to (8) are as follows:

$$\begin{aligned} B(c, a) &= \sqrt{(1-c)^2 - a^4} + \sqrt{(1+c)^2 - a^4}, \\ k(c, a) &= \frac{1}{h(c, a)} = \frac{4c}{B(c, a)^2}, \\ p(c, a) &= \sqrt{\frac{1 - (a^2 - c)^2}{1 - (a^2 + c)^2}}. \end{aligned} \quad (21)$$

In this case $\alpha_2 \leq \cos(\vartheta) \leq \alpha_3$ and the boundary condition at the unclamped ends gives

$$\sqrt{2Cm_p} = f_2(c, a) = \frac{2K[k(c, a)]}{B(c, a)}. \quad (22)$$

The function f_2 at a given a is an increasing function of c . Its minimal value is $f_2(0, a) = \frac{\pi}{2\sqrt{1-a^4}}$. The solution for Cm_p exists if $\sqrt{2Cm_p} > \frac{\pi}{2\sqrt{1-a^4}}$. As a result in the limit $Cm_f \rightarrow 0$ for the critical value of Cm_p^c we have

$$Cm_p^c = \frac{\pi^2}{8} + \frac{2Cm_f^2}{\pi^2}. \quad (23)$$

Relation (23) shows that the remanent magnetization increases the critical magnetoelastic number for the existence of the neutral hairpin configuration. The stability of the neutral solution shown in Fig. 9 is investigated by both the semianalytical and the numerical methods. For the values of the magnetoelastic numbers $Cm_p = 1.53$, $Cm_f = 0.03$, both methods for the negative eigenvalue give $\lambda = -1.96$. Thus the hairpin configuration is unstable. In Ref. [7] this instability for propelling a filament with the hairpin shape was stabilized by reducing the bending modulus in its central part.

IV. CONCLUSIONS

Magnetic rods with remanent magnetization and finite paramagnetic susceptibility in an applied field possess quite a rich family of equilibrium shapes, the morphology of which may be classified by two magnetoelastic numbers. In the standard cases used in magnetic soft matter experiments the rods have unfixed and unclamped ends which are unstable, in agreement with the analysis carried out here. The two methods we have proposed allow us to analyze the stability

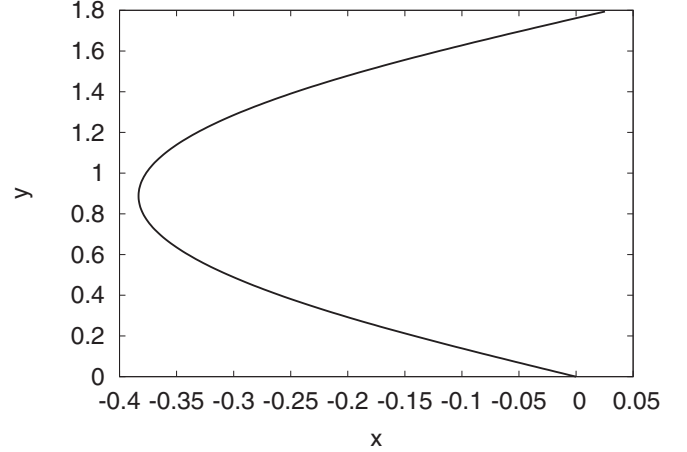


FIG. 9. Neutral hairpin solution. $Cm_p = 1.53$, $Cm_f = 0.03$.

of particular equilibrium configurations even though a general analysis is still lacking.

ACKNOWLEDGMENT

The authors acknowledge support by Scientific Council of Latvia Grant No. lzp-2020/1-0149. We are thankful to R. Livanovics for discussions.

APPENDIX: EIGENVALUE PROBLEM

The first method is based on an integral representation of the solution and consideration of two Cauchy problems. Putting Eq. (16) in the form

$$\frac{d^2 \delta \vartheta}{dl^2} + \lambda \delta \vartheta = Q \delta \vartheta, \quad (A1)$$

and introducing the Green's function of the boundary problem

$$\frac{d^2 G(l, \tau)}{dl^2} + \lambda G(l, \tau) = \delta(l - \tau), \quad \left. \frac{dG}{dl} \right|_{l=\pm 1} = 0, \quad (A2)$$

the problem is reduced to the solution of the integral equation

$$\delta \vartheta(l) = \int_{-1}^1 G(l, \tau) Q(\tau) \delta \vartheta(\tau) d\tau, \quad (A3)$$

where

$$\begin{aligned} G &= \frac{\cos[\sqrt{\lambda}(l-1)] \cos[\sqrt{\lambda}(\tau+1)]}{\sqrt{\lambda} \sin(2\sqrt{\lambda})}, \quad l > \tau, \\ G &= \frac{\cos[\sqrt{\lambda}(\tau-1)] \cos[\sqrt{\lambda}(l+1)]}{\sqrt{\lambda} \sin(2\sqrt{\lambda})}, \quad l < \tau. \end{aligned} \quad (A4)$$

Equation (A3) may be rewritten as follows:

$$\begin{aligned} \delta \vartheta(l) &= \frac{\cos[\sqrt{\lambda}(l+1)] \int_{-1}^1 \cos[\sqrt{\lambda}(\tau-1)] Q(\tau) \delta \vartheta(\tau) d\tau}{\sqrt{\lambda} \sin(2\sqrt{\lambda})} \\ &+ \frac{1}{\sqrt{\lambda}} \left(\sin(\sqrt{\lambda}l) \int_{-1}^l \cos(\sqrt{\lambda}\tau) Q(\tau) d\tau \right. \\ &\quad \left. - \cos(\sqrt{\lambda}l) \int_{-1}^l \sin(\sqrt{\lambda}\tau) Q(\tau) d\tau \right). \end{aligned} \quad (A5)$$

After some transformations we have

$$\begin{aligned}\delta\vartheta(+1) &= \frac{\cos(\sqrt{\lambda})c_1(\lambda) - \sin(\sqrt{\lambda})c_2(\lambda)}{\sqrt{\lambda}\sin(2\sqrt{\lambda})}, \\ \delta\vartheta(-1) &= \frac{\cos(\sqrt{\lambda})c_1(\lambda) + \sin(\sqrt{\lambda})c_2(\lambda)}{\sqrt{\lambda}\sin(2\sqrt{\lambda})},\end{aligned}\quad (\text{A6})$$

where

$$\begin{aligned}c_1(\lambda) &= \int_{-1}^1 \cos(\sqrt{\lambda}\tau)Q(\tau)\delta\vartheta(\tau)d\tau, \\ c_2(\lambda) &= \int_{-1}^1 \sin(\sqrt{\lambda}\tau)Q(\tau)\delta\vartheta(\tau)d\tau.\end{aligned}\quad (\text{A7})$$

To find c_1, c_2 we consider two Cauchy problems for Eq. (A1). The first Cauchy problem for Eq. (A1) is formulated as

follows: $h_p(-1) = 1, dh_p/dl(-1) = 0$. We denote $f_p(\lambda) = h_p(1, \lambda)$. Then from the unity of the ODE solution, $h(l) = h_p(l)\delta\vartheta(-1)$ is the eigenfunction. As a result, $\delta\vartheta(+1) = f_p\delta\vartheta(-1)$. In similar way the second Cauchy problem is formulated: $h_m(1) = 1, dh_m/dl(1) = 0$. Denoting $f_m(\lambda) = h_m(-1, \lambda)$ we see that $h = h_m(l)\delta\vartheta(1)$ is the eigenfunction. Then $\delta\vartheta(-1) = f_m\delta\vartheta(1)$ and as a result the following set of equations for c_1, c_2 is obtained:

$$\begin{aligned}(f_p - 1)\cos(\sqrt{\lambda})c_1 + (1 + f_p)\sin(\sqrt{\lambda})c_2 &= 0, \\ (1 - f_m)\cos(\sqrt{\lambda})c_1 + (1 + f_m)\sin(\sqrt{\lambda})c_2 &= 0.\end{aligned}\quad (\text{A8})$$

The condition of the solvability of Eqs. (A8) gives the following equation for the eigenvalues:

$$f_p(\lambda)f_m(\lambda) = 1. \quad (\text{A9})$$

-
- [1] C. Goubault, P. Jop, M. Fermigier, J. Baudry, E. Bertrand, and J. Bibette, Flexible Magnetic Filaments as Micromechanical Sensors, *Phys. Rev. Lett.* **91**, 260802 (2003).
- [2] A. Koenig, P. Hebraud, C. Gosse, R. Dreyfus, J. Baudry, E. Bertrand, and J. Bibette, Magnetic Force Probe for Nanoscale Biomolecules, *Phys. Rev. Lett.* **95**, 128301 (2005).
- [3] M. Roper, R. Dreyfus, J. Baudry, M. Fermigier, J. Bibette, and H. A. Stone, On the dynamics of magnetically driven elastic filaments, *J. Fluid Mech.* **554**, 167 (2006).
- [4] A. Cebers and K. Erglis, Flexible magnetic filaments and their applications, *Adv. Funct. Mater.* **26**, 3783 (2016).
- [5] J. Ciambella, A. Favata, and G. Tomassetti, A nonlinear theory for fibre-reinforced magneto-elastic rods, *Proc. R. Soc. A* **474**, 20170703 (2018).
- [6] R. Dreyfus, J. Baudry, M. Roper, M. Fermigier, A. A. Stone, and J. Bibette, Microscopic artificial swimmers, *Nature (London)* **437**, 862 (2005).
- [7] A. Cebers, Flexible magnetic swimmer, *Magnetohydrodynamics* **41**, 63 (2005).
- [8] M. Roper, R. Dreyfus, J. Baudry, M. Fermigier, J. Bibette, and H. A. Stone, Do magnetic micro-swimmers move like eukaryotic cells?, *Proc. R. Soc. A* **464**, 877 (2008).
- [9] K. Erglis, R. Livanovics, and A. Cebers, Three dimensional instability of the flexible ferromagnetic loop, *Magnetohydrodynamics* **46**, 245 (2010).
- [10] A. Cebers and T. Cirulis, Magnetic elastica, *Phys. Rev. E* **76**, 031504 (2007).
- [11] D. D. Barreto, S. Saxena, and A. Kumar, A magnetoelastic theory for Kirchhoff rods having uniformly distributed paramagnetic inclusions and its buckling, *Int. J. Solids Struct.* **234–235**, 111147 (2022).
- [12] A. Zaben, G. Kitenbergs, and A. Cebers, Instability caused swimming of ferromagnetic filaments in pulsed field, *Sci. Rep.* **11**, 23399 (2021).